

ELECTROMAGNETIC INDUCTION HEATING OF TP-CFRP LAMINATES: FEM MODELLING AND VALIDATION

W.J. Vankan¹, N. van Hoorn¹, A.J. de Wit¹, and T.P.A. Koenis¹

¹ Royal Netherlands Aerospace Centre NLR, Aerospace Vehicles Division, Collaborative Engineering Systems
Department, Anthony Fokkerweg 2, 1059 CM Amsterdam, The Netherlands

e-mail: jos.vankan@nlr.nl

Abstract

Accelerated adoption of new and innovative aircraft technologies is necessary to achieve the long-term goals for global aviation towards net-zero carbon emissions by 2050. Many of these innovative technologies are already being investigated. One of these technologies is the application of advanced thermo-plastic (TP) carbon fiber reinforced polymer (CFRP) composite components for light-weight airframe assemblies. The correct implementation of the related innovative material and manufacturing technologies is only possible if accurate predictions of the implications of these technologies can be made. For that purpose, advanced modelling and simulation methodologies are indispensable. For example, the use of advanced 3D finite element method (FEM) modelling is essential for the prediction and understanding of complex local electromagnetic (EM) inductive heating phenomena in composite laminates. Such EM simulations can support induction welding (IW) processes that can be used in the innovative manufacturing and assembly of TP CFRP composite components. This paper presents an efficient modelling and simulation approach for the EM inductive heating of TP CFRP laminates. Besides the EM phenomena in the laminate, also the thermal phenomena including conduction, convection and radiation play a key role in the inductive heating process. Dependencies of the various properties and parameters in the simulations are presented and explained. Moreover, a comparison is made of the simulation results with experimental results.

Keywords: induction welding, TP-CFRP, Joule heating, thermal analysis, Multidisciplinary Design Optimization

1. Introduction

Aviation is responsible for about 2% of global CO² emissions [1] and has potentially an even larger contribution in total green-house gas (GHG) emissions and anthropogenic global warming. ICAO recognizes the accelerated adoption of new and innovative aircraft technologies as one of the key measures for CO² emissions reduction [2]. These new technologies are necessary to achieve the long-term goals for global aviation towards net-zero carbon emissions by 2050. Many of these innovative technologies are already being investigated. For example, new materials and structures technologies are aiming for lighter airframe structures with better properties for manufacturability and environmental footprint. More specifically, advanced thermo-plastic (TP) carbon fiber reinforced polymer (CFRP) composites are being investigated for their improved light-weight potential, their faster production and assembly processes, and their possibilities for recycling [3].

The correct implementation of the related innovative material and manufacturing technologies is only possible if accurate predictions of the implications of these technologies can be made. For that purpose, advanced modelling and simulation methodologies are indispensable. For example, the use of advanced 3D finite element method (FEM) modelling is essential for the prediction and understanding of complex local electromagnetic (EM) inductive heating phenomena in composite

laminates. Such EM simulations support the induction welding (IW) processes that can be used in the innovative manufacturing and assembly of TP CFRP composite components.

This paper presents an efficient modelling and simulation approach for the EM inductive heating of TP CFRP laminates. Besides the EM phenomena in the laminate, also the thermal phenomena including conduction, convection, and radiation play a key role in the inductive heating process. Dependencies of the various properties and parameters in the simulations are presented and explained. Moreover, a comparison is made of the simulation results with experimental results. The investigations behind these example applications have been executed in the Clean Sky 2 project STUNNING [4] and in the Clean Aviation project FASTER-H2 [5].

2. Electromagnetic Fem Modelling For Induction Welding

In the assembly of light-weight aircraft structures, TP CFRP composite laminates are increasingly utilized. These TP composites can be locally re-melted, allowing them to be joined via welding. An example of an innovative joining technique is welding by local electromagnetic inductive heating, so-called induction welding. Several heating mechanisms take place in the inductive heating of TP CFRP. The extent in which each mechanism contributes to the heating process, depends on the composite material that is heated and the electromagnetic induction process parameters that are applied. At present, the inductive heating of woven fabric composites is well documented and understood [6]. However, the inductive heating of Uni-Directional (UD) ply CFRP laminates is much less understood. According to [7] this could be due to the obstruction of current returning paths within the UD ply that are required for the inductive eddy currents, which are responsible for the main heating mechanism.

In this paper we present a 3D electromagnetic simulation model that can predict the 3D energy source field from local Joule heating due to induced electric currents in the CFRP laminate. This electromagnetic model can be coupled to 3D thermal simulation models that can provide insight into the actual heating of TP CFRP laminate. Specific aspects that are addressed in these simulations include the influence of the UD plies, their orientations and their stacking sequence in the laminate on the eddy current generation and heat generation inside the CFRP laminate that is placed in an electromagnetic field that is induced by an electric coil.

To investigate the detailed behavior of the induced electric currents in the CFRP laminate, we consider a simplified electromagnetic inductive heating experimental set-up, Figure 1. In this set-up we use a large, more or less rectangular water-cooled tubular copper coil with a straight leg just above the laminate, where it generates a relatively simple and well-defined electromagnetic field.

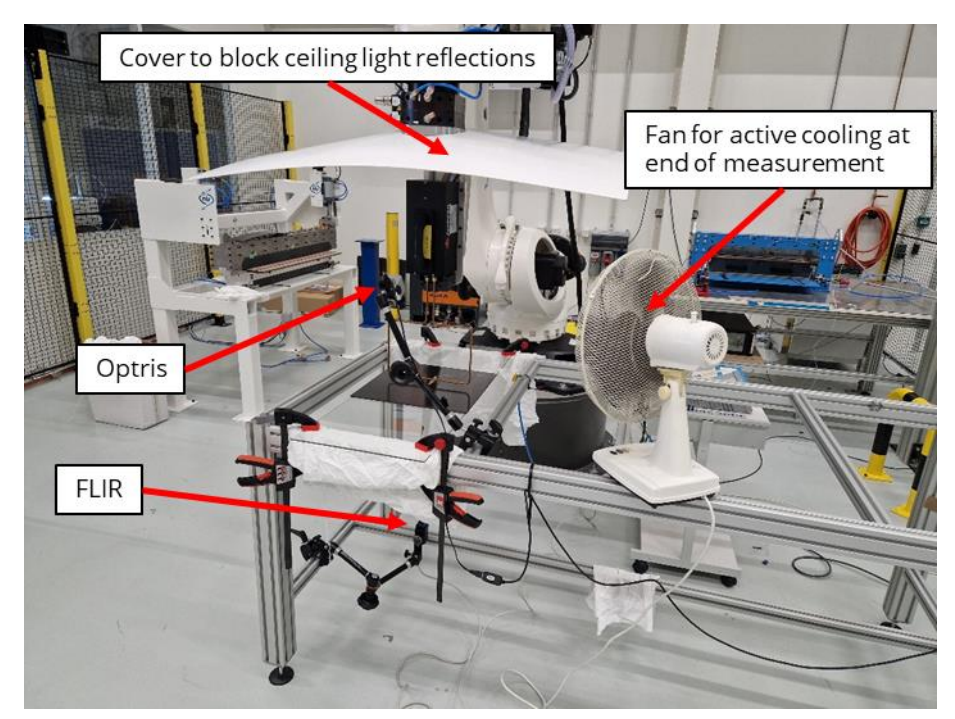


Figure 1 - Illustration of the simplified induction heating experimental setup with the large, more or less rectangular water-cooled tubular copper coil (brown wire) in the middle, with its straight leg just above the laminate (black plate). The infrared thermal measurement equipment (i.e. the Optris and FLIR infrared cameras) are positioned to measure temperatures at the top and bottom surfaces of the laminate.

The laminate size is 130 mm by 400 mm. The coil is located about 14 mm above the laminate. The experimental set-up is shown in some more detail in Figure 2(b). The same simplified experimental set-up has been defined in a FEM electromagnetic simulation model [8], which is implemented in the FEM software Simulia-Abaqus [9], see Figure 2(c), (d).

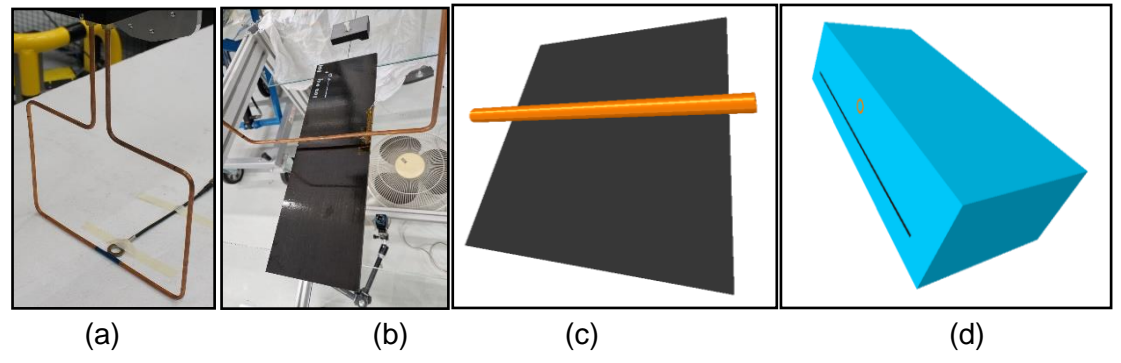


Figure 2 - Illustration of the simplified experimental set-up and its implementation in a FEM electromagnetic simulation model. From left to right, it is shown: (a): the more or less rectangular copper coil; (b): the straight leg of the coil (orange tube) just above the laminate (black plate); (c): the FEM simulation model of the straight horizontal leg of the coil (orange) and the laminate (black); (d) the right half of the model domain, where also (a part of) the air is indicated in blue.

For modelling efficiency, the simulation domain is discretized by a fully-block-structured grid of hexahedral elements (EMC3D8) with parametric mesh refinements in the laminate and the coil. A parametric modelling procedure has been implemented in Matlab [13]. The block-structured hexahedral mesh leads to a simplified rectangular cross-section approximation of the tubular coil with circular cross-section, see Figure 3, but the square cross-section coil in the model has the same cross-sectional area of 16.81 mm² as the circular cross-section coil in the experiment.

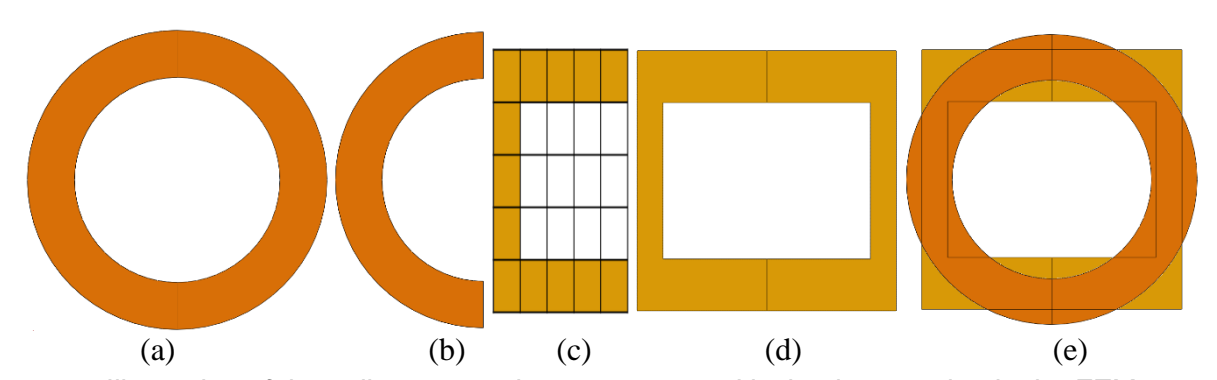


Figure 3 - Illustration of the coil cross-section geometry and its implementation in the FEM electromagnetic simulation model. (a): cross-section of circular coil in experiment, with outer radius 3.175 mm and inner radius 2.175 mm; (b) cross-section of half circular coil that is part of the Q1 domain; (c): cross-section of half square coil, conformal to the hexahedral mesh of the Q1 domain and with the same cross-sectional area as the half circular coil; (d): cross-section of the whole square coil; (e) comparison of the cross-sections of the whole circular and square coils.

Also for modelling efficiency, the FEM electromagnetic simulation model can have a double planar symmetry in the two vertical center-planes: one perpendicular to the coil and one through the center-line of the coil. This symmetry is the case if the cross-ply laminate has only 0- and/or 90-degree plies that are oriented parallel and perpendicular to the coil center-line. In that case only one quadrant of the domain needs to be considered in the simulation model, see **Error! Reference source not found.**; in all other cases the full domain shall be considered.

The volumes of air that are included in the modelling domain around the laminate and the coil are parametrically defined. These surrounding air volumes must not be made too small because then the EM results in the laminate are affected, but should be about 10 times the characteristic length scale associated with the coil/workpiece assembly which is about 25 mm in the considered set-up. From parametric evaluations it is found that air volumes of at least about 250 mm below the laminate and above the coil are required, and air volumes of at least about 10 mm around the sides of the laminate are required. This leads to a Q1-quadrant model domain of about 75 mm by 210 mm by 525 mm in x,y,z-directions, as shown in **Error! Reference source not found.** (c).

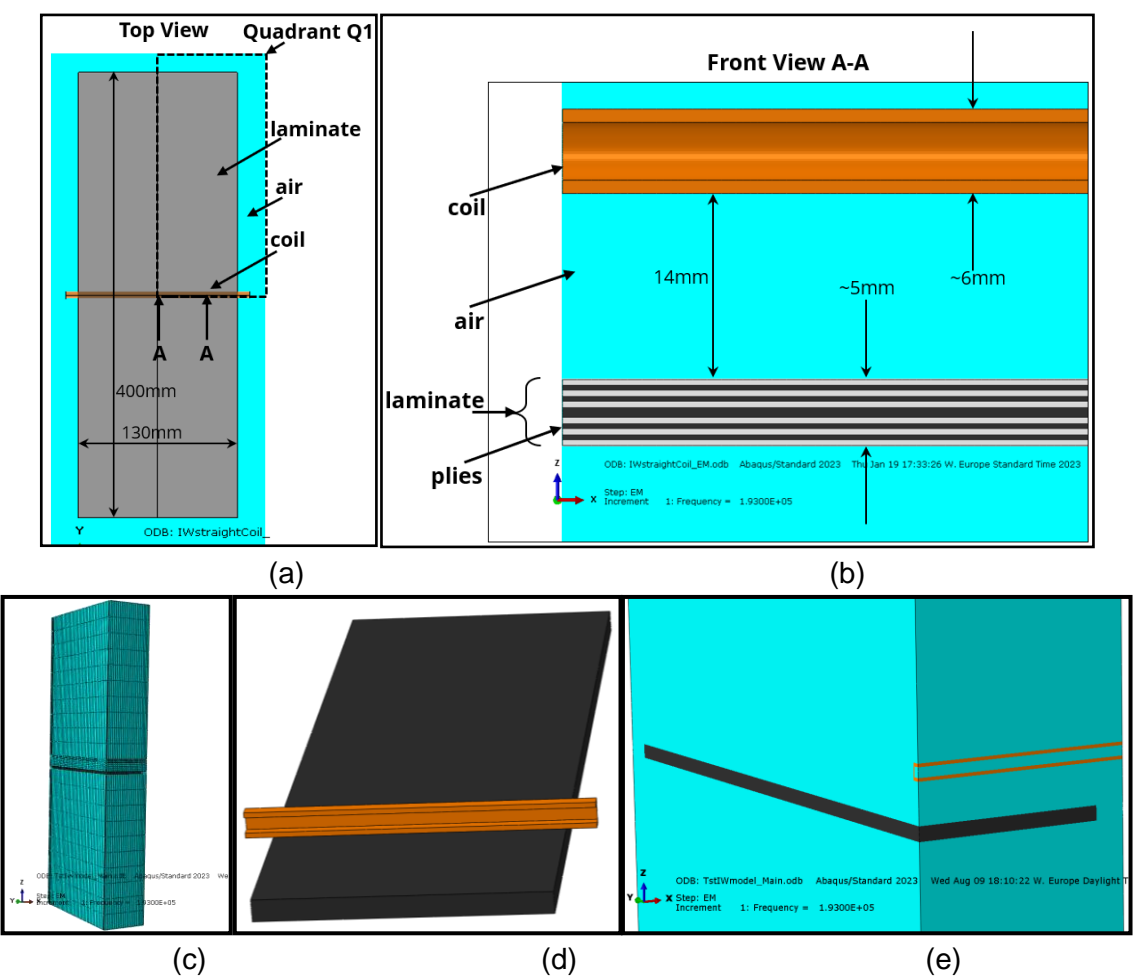


Figure 4 - Illustration of the model domain and the Q1-quadrant fully-block-structured mesh implementation in the FEM electromagnetic simulation model. (a): top-view of the coil and laminate and indication of the Q1 quadrant; (b) front-view of the vertical cross-section in the center-line of the coil; (c): the block-structured hexahedral mesh of the Q1 model domain, where the air is indicated in blue; (d): the FEM simulation model of the straight horizontal leg of the coil (orange) and the laminate (black); (e) the Q1 model domain including air (blue) and zoomed in on the region with the coil (orange) and the laminate (black).

As indicated in the **Error! Reference source not found.**, the FEM electromagnetic simulation model contains three different material sections: the copper coil, the composite laminate plies, and the surrounding air [11]. The composite laminate contains consolidated UD plies of the prepreg material Toray TC1320 PEKK AS4D [12]. For the coil standard copper CU-ETP1 – C11040 is assumed, and atmospheric air at sea level is assumed. The electromagnetic properties that must be prescribed for these materials are given in Table 1 [11]. All electromagnetic properties are assumed isotropic except for the conductivity in the plies, which is assumed to be orthotropic with conductivity matrix:

$$\boldsymbol{\sigma}_{ply} = \begin{bmatrix} \sigma_x & 0 & 0\\ 0 & \sigma_y & 0\\ 0 & 0 & \sigma_z \end{bmatrix} \tag{1}$$

where x,y,z refer to the local coordinate system with x in fiber direction, y in cross-fiber direction and z in thickness direction.

Table 1 - The electromagnetic properties that must be prescribed for the 3 different material sections

ELECTROMAGNETIC INDUCTION HEATING OF TP-CFRP LAMINATES

in the FEM electromagnetic simulation model. For the coil, an electric conductivity of 1.0 S/m is used in the simulations to simplify the prescribed current density and avoid substantial self-inductance effects in the coil.

	Electric conductivity [S/m]	Magnetic permeability [H/m]	Dielectric constant (Electrical Permittivity) [F/m]
Air	1.0	1.26E-6	8.85E-12
Coil	1.0 (60.0E6)	1.26E-6	8.85E-12
Ply	fiber direction: σ_x =33500.0	1.26E-6	8.85E-12
	cross-fiber direction: σ_y =1.0		
	thickness direction: σ_z =1.0		

With the composite ply properties, the various plies and their thicknesses and orientations can be easily defined for any laminate in the FEM electromagnetic simulation model. A solid FEM mesh with HEX elements is used, where typically each ply is modelled by one or more layers of elements in thickness direction. Typical TP CFRP ply thicknesses are in the order of 0.1 mm so an element thickness of about 0.05-0.1 mm is needed. With an element aspect ratio of 20 this would require an in-plane element size of about 1.0 mm. The typical size of the 3D domain for the FEM electromagnetic simulation is in the order of 100 mm in each direction. This would require for the laminate an in-plane meshing of about 100x100 elements, i.e. 20.000 elements per ply if just 2 elements per ply in thickness direction would be used. Moreover, the mesh of the coil must be reasonably detailed, e.g. contain at least 5 elements in both directions of its cross-section, which has a size of about 5.7 mm by 5.7 mm in global y-z-directions. In the fully-block-structured grid, the mesh of the air directly depends on these element sizes in the laminate and the coil. So, the FEM problem size for the fully discretized 3D domain can grow quite large if a laminate with many plies is considered.

In this paper we consider a Q1 quadrant domain of approximately 75 mm by 210 mm by 525 mm in the x-y-z-directions, respectively. The laminate size in this Q1 quadrant is 65 mm by 200 mm with 36 plies with total thickness of about 5 mm and 2 elements per ply are used in thickness direction. The total domain is discretized into 119952 linear 8 node HEX elements of type EMC3D8 [9]. A symmetric [0,90]-cross-ply composite laminate layup is considered with ply thickness of 0.138 mm and 36 plies with ply angles: [90₃,0₃]_{3s},see Figure 5. Homogeneous Dirichlet boundary conditions are prescribed on the y-z-symmetry plane and on all the outer air surfaces. On the x-z-symmetry plane homogeneous Neumann boundary conditions are applied implicitly. With this relatively small EM simulation model, the model size is limited to 754550 equations and computation time is limited to about 182 CPU seconds on a standard PC.

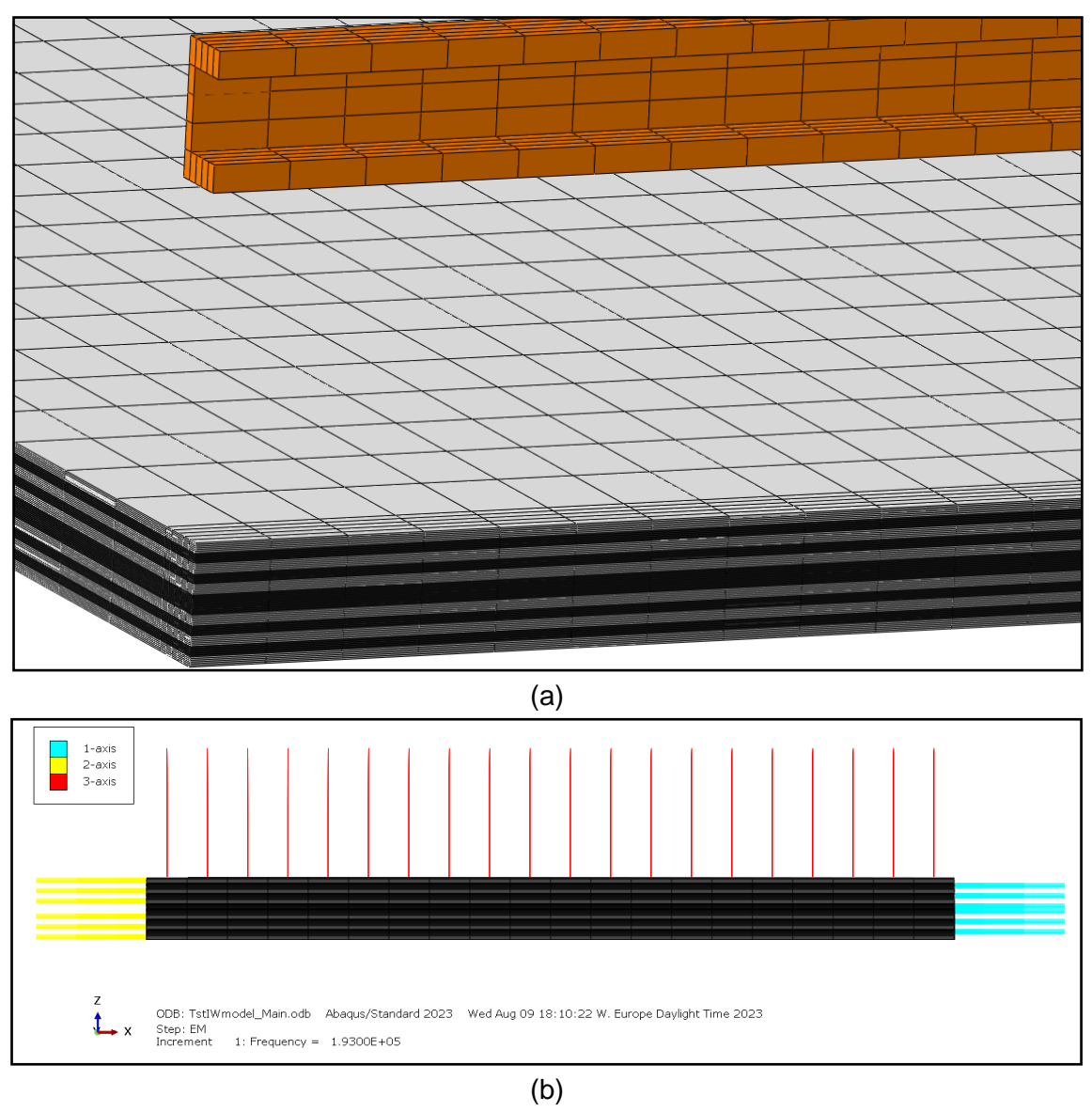


Figure 5 - Illustration of the FEM electromagnetic simulation model. (a): iso-view on the mesh of the considered Q1 domain showing only the coil (orange) and laminate (black, white), where the black layers indicate the 0-degree plies (i.e., parallel to coil) and the white layers indicate the 90-degree plies. (b): Front view in +Y direction on the x-z-symmetry plane of the domain through the center line of the coil, where the element orientation vectors of the plies in the laminate are shown, and the blue lines (1-axis) correspond to the fiber orientations.

In the induction heating experiment, an Alternating Current (AC) of 199.5 A and 193 kHz has been specified in the induction coil. The induction heating equipment (Ambrell EASYHeat 83100 LI [10]) has a controller that maintains the coil current at the correct value, taking care of potentially varying self-induction effects due to the properties of the heated specimen and the environment around the coil. The actual AC current in the coil is a multi-periodical signal with high frequency of 193 kHz combined with lower frequency components; see the small signal sample of the actual AC current in the coil in Figure 6. For the actual AC current in the coil it is derived that the root mean square (RMS) value of the current is about 199.5 A, which is more or less equal to the AC current indication of 199.5 A that is given by the controller of the induction heating equipment. This indicates that the 199.5 A is the coil current's RMS value, i.e. the amplitude of a corresponding perfectly sinusoidal coil current as is used in the FEM model- would be 199.5 A* $\sqrt{2}$ =282.1 A.

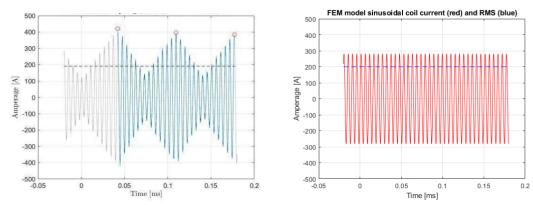


Figure 6 - Illustration of a small sample of the actual measured AC current in the coil of the experiment (left), which is a multi-periodical signal with high frequency of 193 kHz combined with lower frequency components. On the right: the corresponding perfectly sinusoidal coil current as used in the FEM model, with the same RMS value of 199.5 A, and amplitude of 282.1 A.

In the FEM electromagnetic simulation, a constant AC current with a frequency of 193 kHz is prescribed in the coil as a current density (EMCDA in Abaqus) with an amplitude of 16.786 A/mm² (282.1356 A / 16.81 mm²) in length direction of the coil. This directly corresponds to the 193 kHz AC current with the same RMS of 199.5A that is applied to the coil in the experiment. The difference between the periodic current signals in the experiment and in the FEM model is not considered here in further detail. But this difference may cause small differences in induced effects in the laminate due to the slightly different rates of change in the currents.

The coil is placed at a distance of 14 mm above the laminate, that means an air gap of 14 mm exists between the coil and the upper surface of the laminate. The AC current in the coil creates an electromagnetic field in and around the coil. The magnetic induction or flux density (EMB) and the electric (EME) fields are shown in Figure 7.

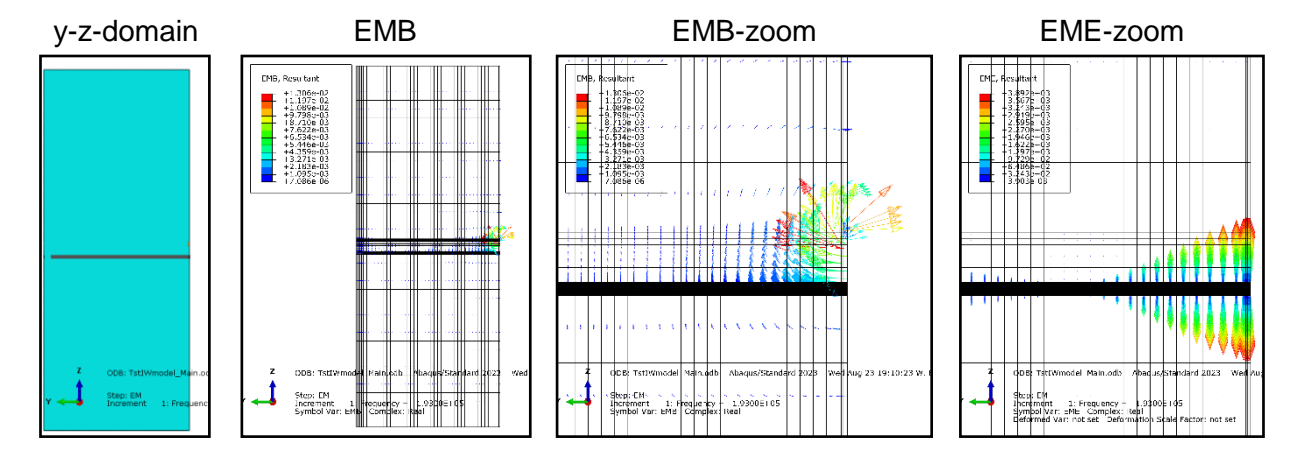


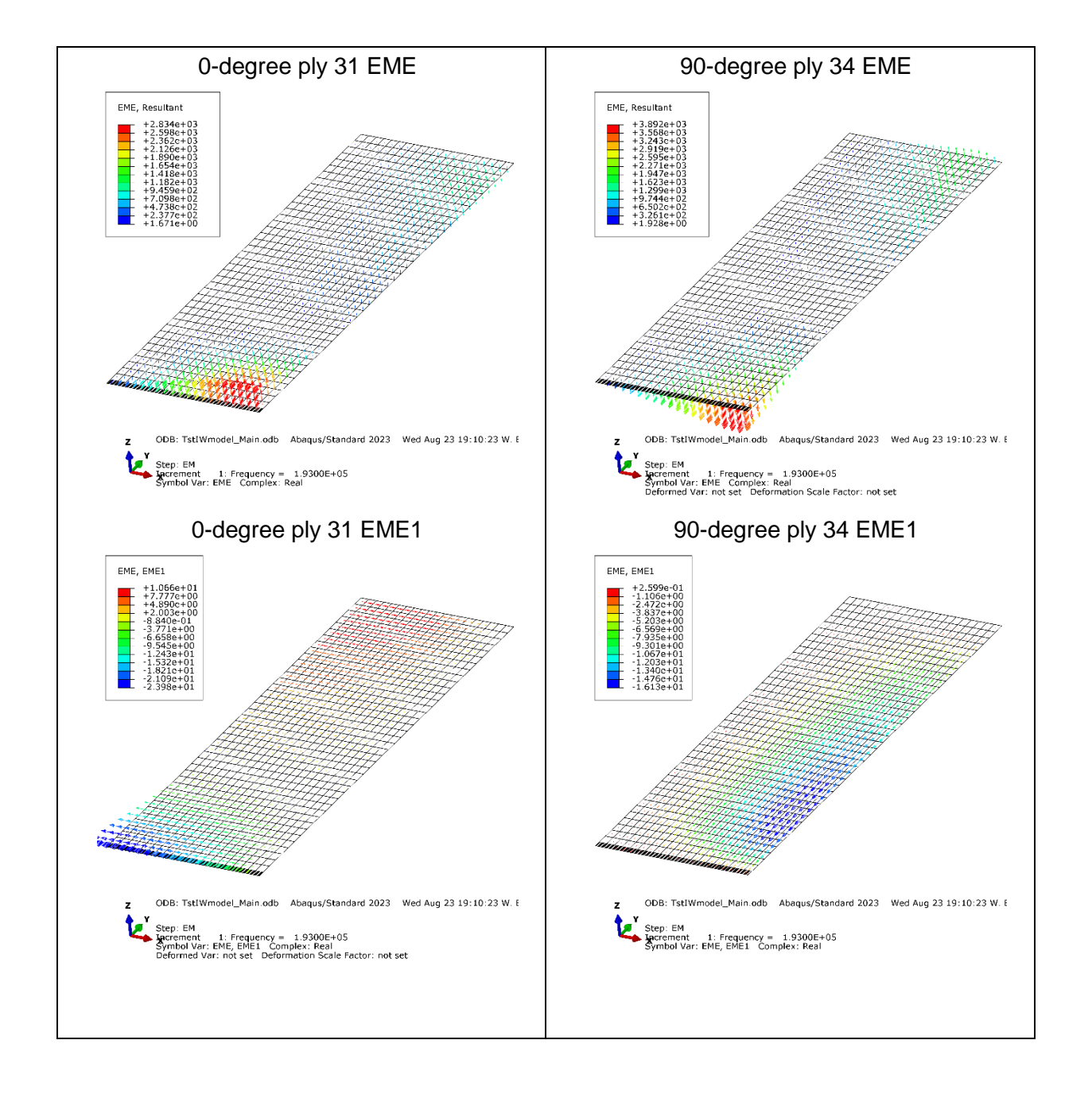
Figure 7 - Illustration of the magnetic induction or flux density (EMB) and the electric (EME) fields in and around the coil. The direction of the EME vector field is upward in certain plies and downward in other plies.

The electromagnetic field around the coil induces eddy currents in the composite laminate. The local strength of these eddy currents is determined by the local strength and orientations of the electromagnetic field (EME) and the local conductivity properties and orientations of the plies in the composite laminate. As indicated in Table 1, the ply conductivity is very high in fiber direction and very low perpendicular to the fibers, which is a result of the very high conductivity of the carbon fibers and very low conductivity of the TP matrix material. Due to these local orientations of the ply

ELECTROMAGNETIC INDUCTION HEATING OF TP-CFRP LAMINATES

conductivities and of the electromagnetic field, very specific patterns of induced currents will appear in the plies. In the FEM electromagnetic simulation these induced currents are calculated as local electromagnetic current density (EMCD) vectors. In the composite laminate the EMCD resultant vectors typically are more or less aligned with the local fiber direction because that is where the highest conductivity exists. We will focus now on the results in the upper six plies of the laminate, i.e. the ply numbers 31-36 from bottom to top with ply angles [0₃,90₃]. These six plies are closest to the coil and have the highest induced currents. In the considered cross-ply laminate the fiber directions in the upper three 90-degree plies are perpendicular to the coil direction, in the three 0-degree plies below the fiber directions are aligned with the coil direction.

For the 0-degree ply, number 31, which has fibers aligned with the coil, we find the highest EME values right below the coil on the right side of the laminate. However, if we look at the absolute values of the x-components of the EME vectors, indicated here as EME1, we find the highest absolute values right below the coil on the left side of the laminate (|EME1|max=23.98 V/m). When multiplied with the local conductivity component (σ_x = 33500.0 S/m), we find for the local x-component of the EMCD vector EMCD1= σ_x ·EME1=33500.0 ·(-23.98)=-803330.0 A/m². This is also the maximum absolute value for the EMCD1 field in the ply 31. Apparently, the EMCD1 is the dominant component of the EMCD vector because the maximum value of the EMCD resultant vector field is also 803330.0 at the same location. Similarly for the 90-degree ply 34, we find for the maximum absolute value of the local x-component of the EMCD vector EMCD1= σ_x ·EME1=33500.0 · (-16.13)=-540355.0 A/m². Also in ply34 this EMCD1 is the dominant component of the EMCD vector because the maximum value of the EMCD resultant vector field is also 5.403E5 A/m² at the same location. See the EME and EMCD vector fields below in Figure 8.



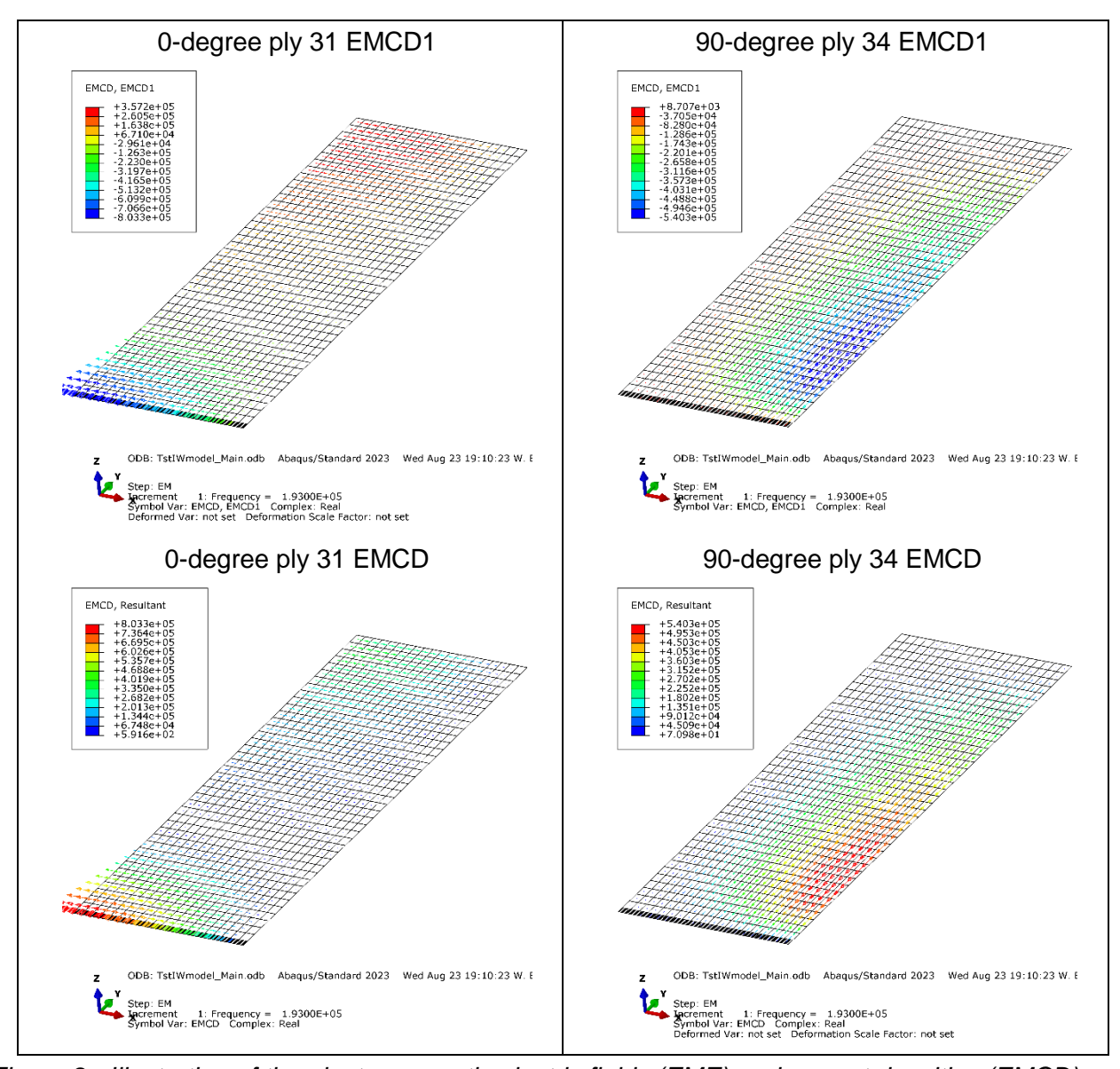
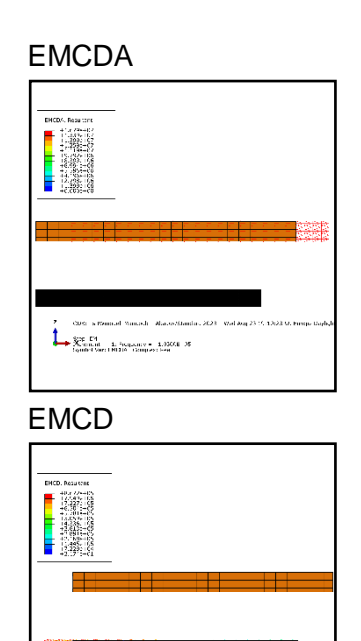


Figure 8 - Illustration of the electromagnetic electric fields (EME) and current densities (EMCD) results in the laminate; left: for the 0-degree ply nr. 31; right: for the 90-degree ply nr. 34. The vector plots show the complex-real part of EMCD and EME solutions.

If we look at the EMCD field in all the upper 3 0-degree plies numbers 31-33, then we find the highest maximum EMCD value of 6.132E5 in the ply number 33, which is closest to the coil. If we look at the EMCD field in all the upper 3 90-degree plies numbers 34-36, then we find the highest maximum EMCD value of 3.821E5 in the ply number 34. See Figure 9. This ply is not the closest to the coil, but it is the closest to an adjacent 0-degree ply. The eddy currents in this ply 34 are a result of the interaction with this adjacent 0-degree ply. In fact, the eddy currents would not even exist if there would be only 0-degree or only 90-degree plies in the laminate. Therefore the eddy currents in the laminate are strongest near the cross-ply interfaces. This effect was also previously investigated by more specific modelling of the cross-ply interfaces [11].

O-degree plies 31-33 EMCD EMCD, Resultant +8.672e+05 +7.949e+05 +7.227e+05 +6.504e+05 +5.781e+05 +5.059e+05 +1.4336e+05 +1.446e+05 +1.446e+05 +1.446e+05 +1.446e+05 +1.446e+05 +1.446e+05 +1.446e+05 +1.446e+05 +1.4536e+01 The property of the property of



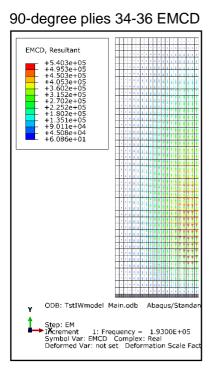


Figure 9 - Illustration of the electromagnetic current densities (EMCD) in the laminate: (a): Top view on the EMCD vectors in the 0-degree plies numbers. 31-33: high EMCD in -X-direction is obvious below the coil, and increased EMCD in +X-direction near the far edge of the laminate in the top of the picture. (b) Front view of coil and laminate in global +Y-direction on the x-z-symmetry plane, showing the pre-scribed current density EMCDA in the coil (top) and the induced current density EMCD in the laminate (bottom); (c): Top view on the EMCD vectors in the 90-degree plies 34-36: high EMCD in -Y-direction occurs along the right edge of the laminate. All the vector plots show the complex-real part of EMCD solution.

SEC E4

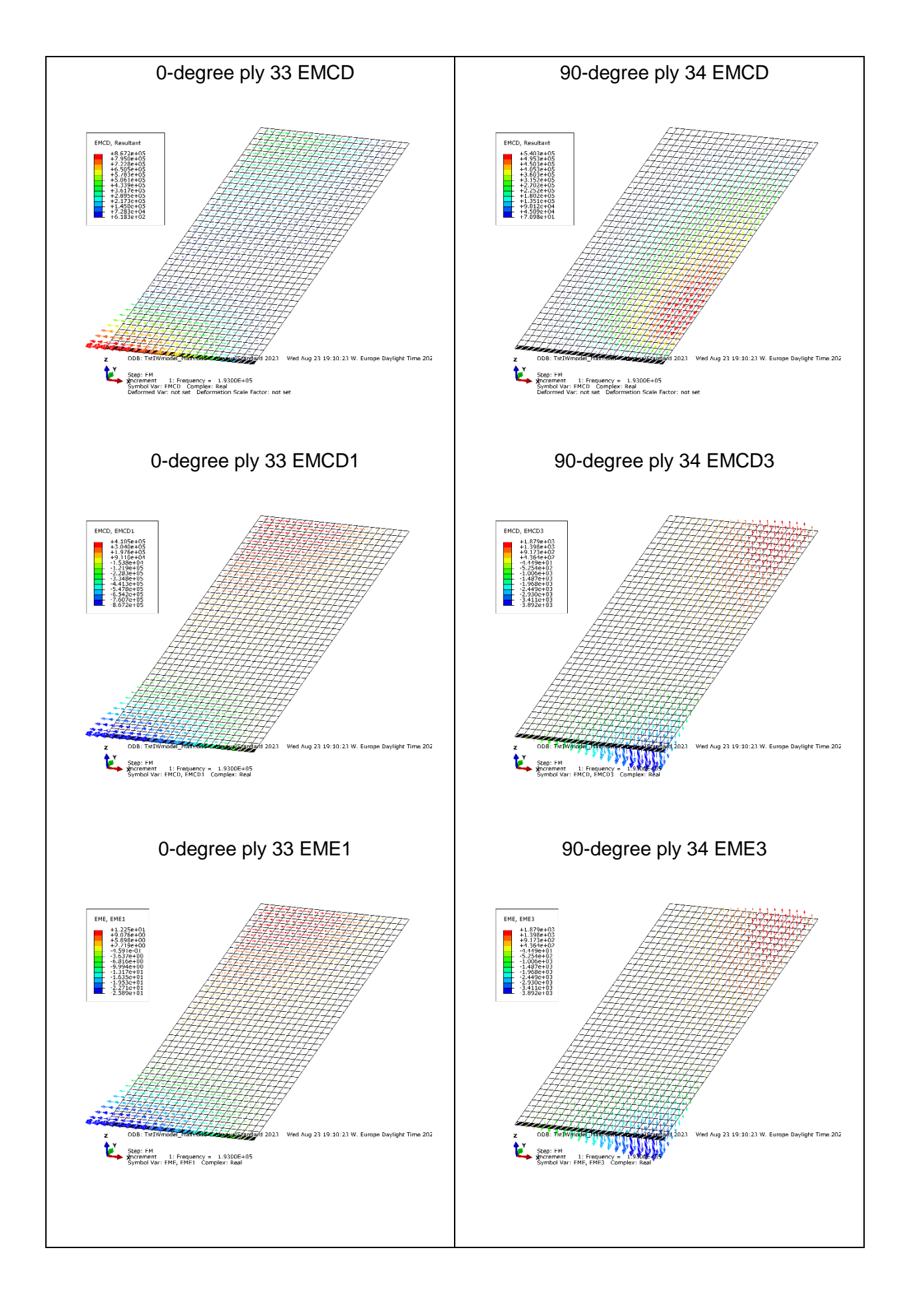
**X min.m 1: Program = 1.03008-08

Londord Sec: 1921 Dampies: Fee

Deformed via:: not sec. Deformet on State Factor:

Because in the 0-degree plies the conductivity in global Y-direction is very low, there are no high return-currents in these plies, i.e. currents that close a loop in the laminate from which a counteracting magnetic field originates. Instead, these high return-currents in +Y- and -Y-directions occur in the adjacent 90-degree plies where the conductivity in global Y-directions is very high, as can be seen from the EMCD vectors in Figure 9. In consequence, increased return-currents in global +X-direction occur again in the 0-degree plies near the edges of the laminate far away from the coil so in relatively low electromagnetic field strength.

The local current densities (EMCD) in the laminate combined with the local electric field strength (EME) contribute to the local Joule heating (EMJH). The areas with the largest coinciding EME and EMCD vector-components have the highest EMJH values. Therefore the local values of EMJH depend strongly on the detailed orientations of the local EME and EMCD vectors. For the ply 33, the major EMJH contribution comes from the EME1 and EMCD1 vector components, see Figure 10 left column. For the ply 34, the major EMJH contribution comes from the EME3 and EMCD3 vector components, see Figure 10 right column.



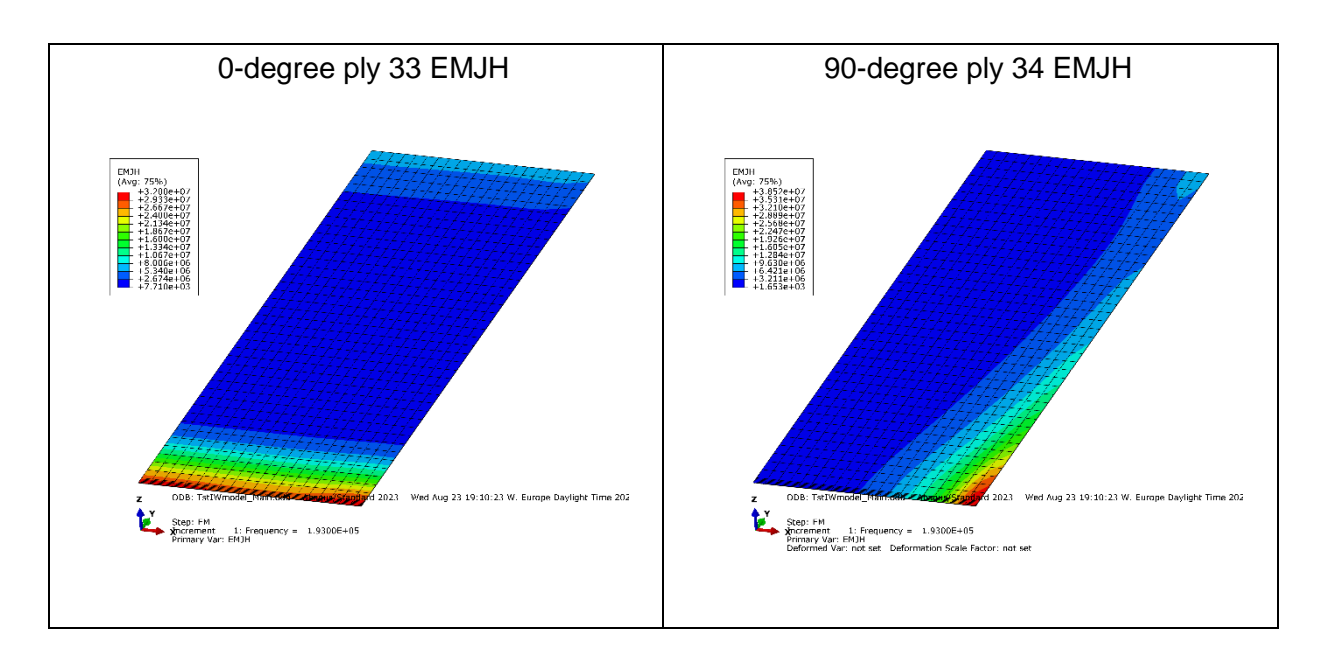


Figure 10 - Illustration of the electromagnetic current densities (EMCD), electric fields (EME) and Joule heating (EMJH) results in the laminate; left: for the 0-degree ply nr. 33; right: for the 90-degree ply nr. 34. The vector plots show the complex-real part of EMCD and EME solutions.

We mirror the EMJH results in the Q1 quadrant to compose the result for the laminate in the whole domain, as shown for the 0-degree ply nr. 33 and the 90-degree ply nr. 34 in Figure 11.

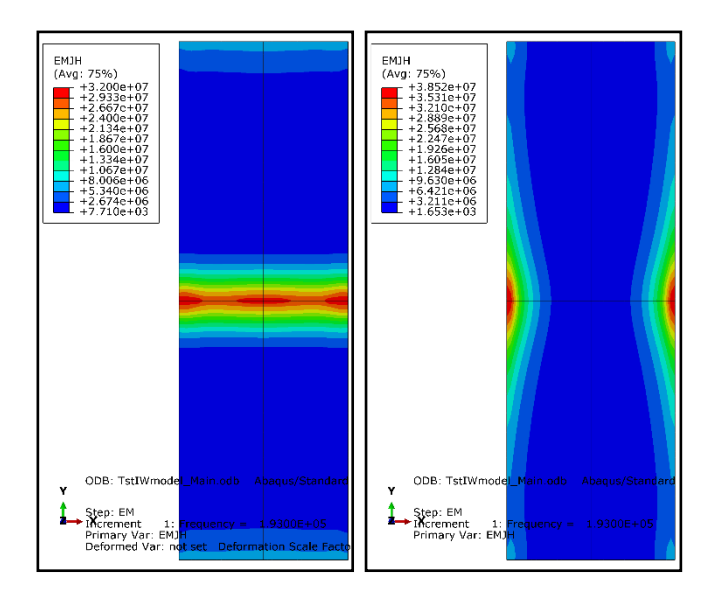


Figure 11 - Illustration of the electromagnetic Joule heating (EMJH) in the laminate. Left: Top view of the EMJH contours in the 0-degree ply nr. 31 in all 4 quadrants of the laminate. Right: Top view of the EMJH contours in the 90-degree ply nr. 34 in all 4 quadrants of the laminate.

3. Thermal Fem Modelling For Induction Welding

A thermal FEM model is defined for the heat transfer analysis of the inductive heating experiment. This thermal model is focused on the laminate because the induction heat sources are located in the plies. The surrounding air is represented in the thermal FEM model by convective and radiative interaction properties at the laminate-air boundaries.

The local EMJH results in the laminate from the electromagnetic simulation can be translated to the energetic source terms in a 3D thermal simulation of the same domain. The EMJH results represent power per unit of volume (i.e., expressed in W/m3) and are element based (i.e., just one value for each whole element). The translation of these EMJH values to the energetic source terms in the 3D thermal simulation must be done conservatively, i.e. the total power in the whole domain for the EMJH result data and for the energetic source term data must be equal. To achieve that, the discretization of the energetic source term data must be balanced: the local values must correspond as good as possible with the local EMJH values, but also in any local volume within the domain the total power must correspond as good as possible. If the mesh in the thermal FEM model is different from the mesh in the electromagnetic model then this must be adequately handled by conservative interpolation methods, e.g. as provided by the Abaqus emloads utility [9] or other dedicated algorithms [14]. In the present thermal FEM model, the mesh is equal to the mesh in the electromagnetic model. This strongly simplifies the conservative translation of the EMJH values. The EMJH value from each electromagnetic element (EMC3D8 [9]) is prescribed as a body heat flux value (*DFLUX, [9]) to each corresponding thermal element (8 node hexahedral element type DC3D8 [9]). In the thermal simulation, the thermal properties of the UD ply material are temperature dependent and are prescribed as given in Figure 12. The laminate's temperature dependent convective interaction properties at the laminate-air boundaries are prescribed as given in Figure 12. The radiative interaction properties at the laminate-air boundaries are constant and have a value of 0.95 at all sides (derived from [15], section 2.6.2.). The natural convection coefficients of the considered laminate depend on the laminate's surfaces size, geometry, direction, and temperature, and the values used here are based on the approach of Moser [15].

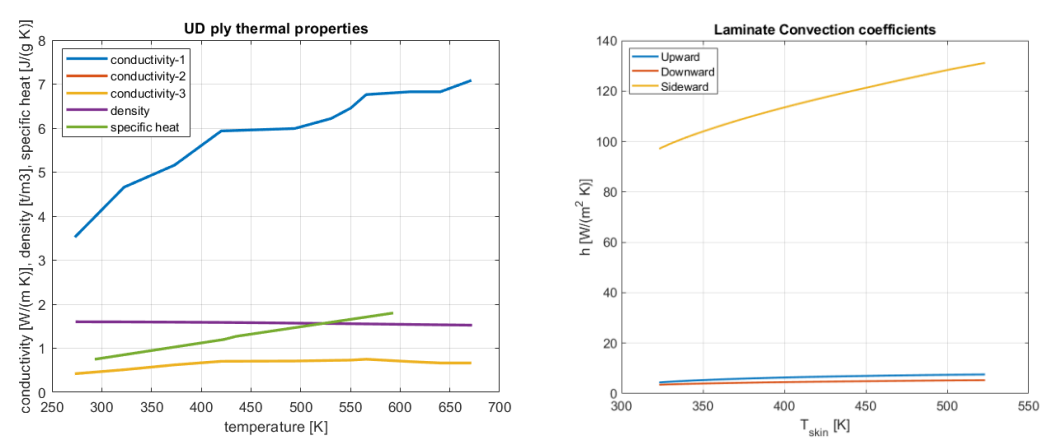


Figure 12 - Illustration of the temperature dependent thermal properties of the UD ply material and convective interaction properties of the laminate as used in the thermal simulation.

This thermal model is used for a heating simulation of the inductive heating experiment described above, in which a continuous heating during 37 seconds has been applied. The resulting temperatures in the top surface of the laminate then can be compared to the measured temperatures in the experiment. These measurements are made with an infrared Optris PI 640 camera, and indicate a heating pattern with maximum temperatures of about 176 °C at the left and right edges of the laminate right below the coil.

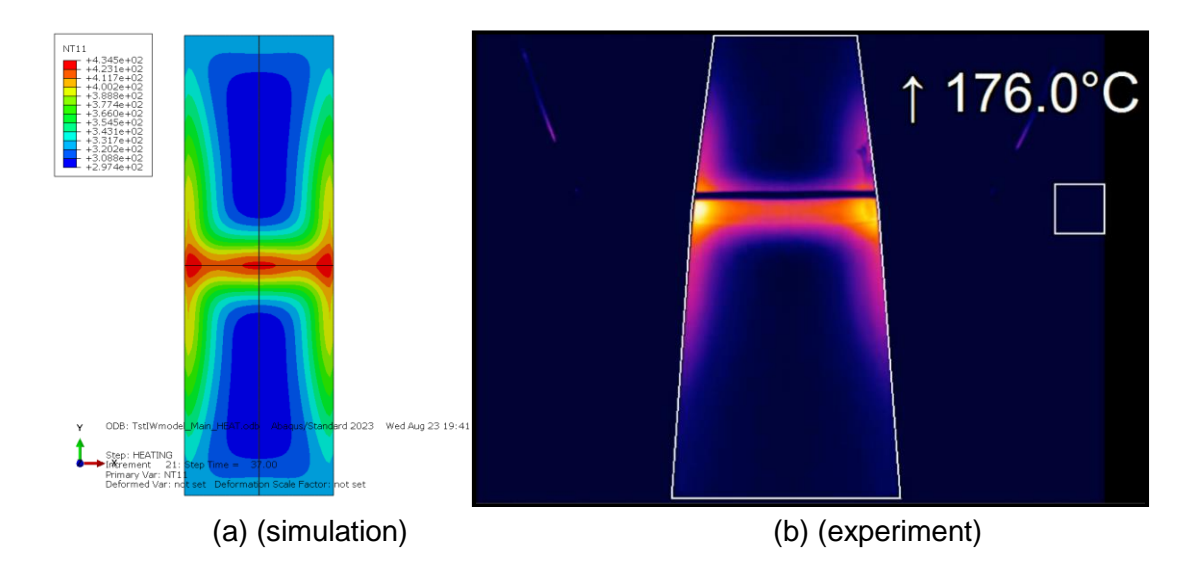


Figure 13 - Comparison of the thermal simulation results for the temperature contour with the measured temperatures in the experiment in the top surface of the laminate after 37s heating. (a): Simulation prediction of the temperature contour (NT11 in Kelvin; max value is around 161 °C) on the top surface of the laminate. (b): Measured temperatures in the experiment on the top surface of the laminate (purple-yellow colors; dark purple: min value: 20 °C; bright yellow: max value: 176 °C).

In the experiment also the cooling of the laminate after heating was measured during 70 seconds. After 37 seconds heating, the coil current was turned off and the heated laminate passively cooled due to conduction, convection and radiation to its environment. After these 70 seconds cooling the resulting temperatures in the top surface of the laminate can be compared to the measured temperatures in the experiment. Also these measurements are made with an infrared Optris PI 640 camera, and indicate the resulting pattern of the cooled laminate with maximum temperatures of about 100 °C at the left and right edges of the laminate right below the coil.

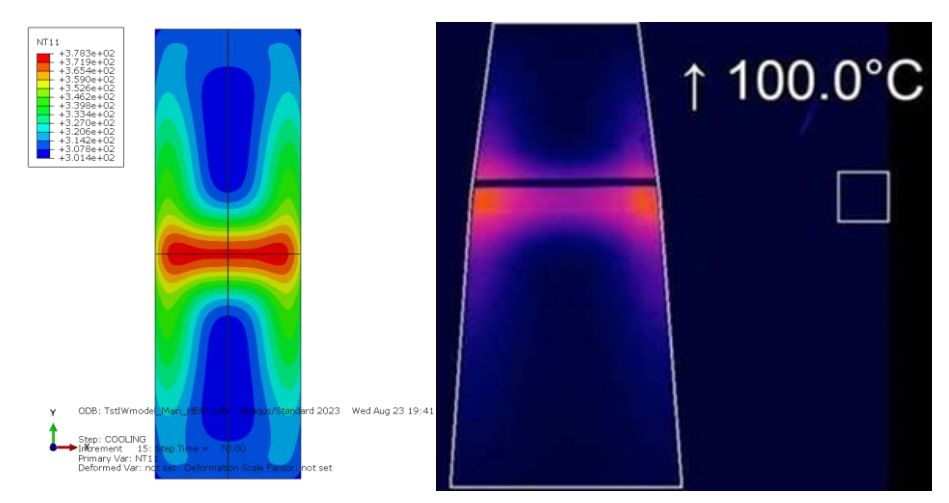


Figure 14 - Comparison of the thermal simulation results for the temperature contour with the measured temperatures in the experiment in the top surface of the laminate after 70s cooling. (a): Simulation prediction of the temperature contour (NT11 in Kelvin; max value is around 105 °C) on the top surface of the laminate. (b): Measured temperatures in the experiment on the top surface of the laminate (purple-yellow colors; dark purple: min value: 20 °C; bright yellow: max value: 100 °C).

It is found that the temperature contours match reasonably well, see Figure 13 and Figure 14. Especially the global predicted temperature distribution on the laminate surface is predicted reasonably accurate. The predicted peak temperature values after 37 seconds heating appear to be

about 15 °C too low in comparison to the experiment (Figure 15). The predicted peak temperature values after 70 seconds cooling appear to be about 5 °C too high in comparison to the experiment. There may be various explanations for these differences. Firstly, differences may be caused by different induced effects in the laminate due to the slightly different rates of change in the coil currents of the experiment and of the FEM model. This is because the current in the experiment is governed by the induction welding equipment controller and not sinusoidal, whereas the current in the FEM is sinusoidal. Secondly, differences may be caused by the thermal conductivity values of the laminate, which are currently not accurately known and should be determined in more detail.

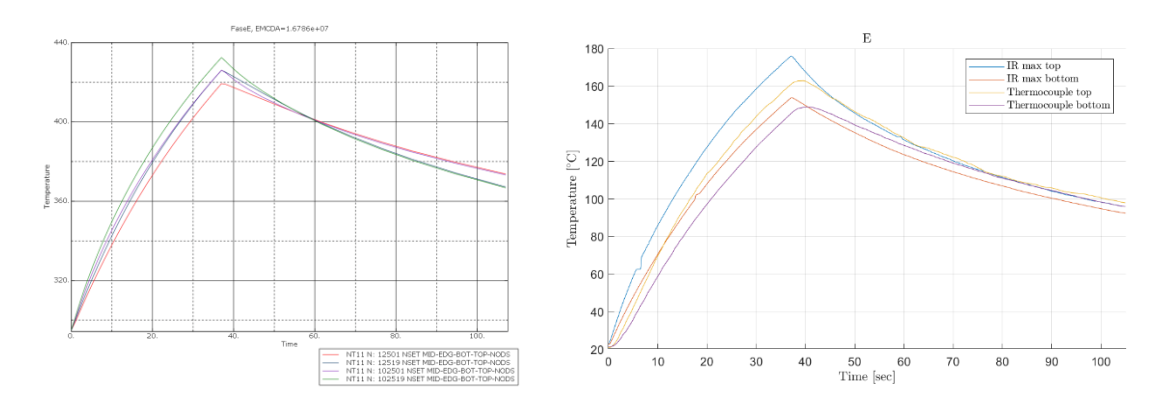


Figure 15 - Comparison of the time-transient thermal simulation results for the temperature values with the measured temperatures in the experiment. The temperatures are given at the top and bottom of the laminate in the center and near the edges of the laminate right below the coil. (a): Simulation prediction of the temperature contour (NT11 in Kelvin; max value is around 105 °C) on the top surface of the laminate. (b): Maximum temperatures in the experiment on the top and bottom surfaces of the laminate measured by IR camera's and by thermocouple sensors below the coil near the right edge of the3 laminate.

4. Conclusions

Advanced modelling and simulation methodologies are indispensable for successful application of innovative technologies and radical innovations in modern aviation. An example application has been presented where the development of innovative technologies is supported by increasingly digitalized methods, tools and technologies. In particular, advanced FEM modelling and EM- and thermal analysis have been shown for application to induction welding of TP-CFRP structures.

An efficient 3D modelling and simulation approach for the EM inductive heating of TP CFRP laminates has been presented. Besides the EM phenomena in the laminate, also the thermal phenomena including conduction, convection and radiation play a key role in the inductive heating process. Dependencies of the various properties and parameters in the simulations are presented and comparisons of the simulation results with experimental results have been made. It is found that the major EM and thermal phenomena are captured reasonably well by the simulations. But this is achieved on a strongly simplified test case and induction welding of more complex geometries and laminates will require more modelling an validation efforts.

Therefore further work is needed to enhance these modelling and simulation methodologies and their adoption in standard aeronautic development processes.

Contact Author Email Address

mailto: jos.vankan@nlr.nl

Copyright Statement

The authors confirm that they, and/or their company or organization, hold copyright on all of the original material included in this paper. The authors also confirm that they have obtained permission, from the copyright holder of any third party material included in this paper, to publish it as part of their paper. The authors confirm that they give permission, or have obtained permission from the copyright holder of this paper, for the publication and distribution of this paper as part of the ICAS proceedings or as individual off-prints from the proceedings.

Acknowledgements

The STUNNING project has received funding from the Clean Sky 2 Joint Undertaking (JU) under grant agreement No 945583. The FASTER H2 project has received funding from the Clean Aviation Joint Undertaking (CAJU) under grant agreement No 101101978 (FASTERH2 project). The Clean Sky 2 JU receives support from the European Union's Horizon 2020 research and innovation programme and the Clean Sky 2 JU members other than the Union. The CAJU receives support from the European Union's Horizon Europe research and innovation programme and the CAJU members other than the Union.

Disclaimer

The results, opinions, conclusions, etc. presented in this work are those of the author(s) only and do not necessarily represent the position of the Clean Sky 2 JU nor of the CAJU; the Clean Sky 2 JU and CAJU are not responsible for any use made of the information contained herein.





References

- [1] IEA. https://www.iea.org/energy-system/transport/aviation.
- [2] ICAO. https://www.icao.int/environmental-protection/Documents/Assembly/Resolution_A41-21_Climate_change.pdf.
- [3] Clean Aviation Joint Undertaking. *The next generation Multifunctional Fuselage Demonstrator*—leveraging thermoplastics for cleaner skies, https://www.clean-aviation.eu/sites/default/files/2021-10/CLEAN_SKY_Article_MultiFuse.pdf, 2021.
- [4] STUNNING project. https://www.nlr.org/news/nlrs-stunning-project-departs-for-next-generation-composite-planes/.
- [5] FASTER-H2 project. https://cordis.europa.eu/project/id/101101978.
- [6] Yousefpour A, Hojjati M, and Immarigeon JP. Fusion Bonding/Welding of Thermoplastic Composites, *Journal of thermoplastic composite materials*, 17:303, 2004.
- [7] Ahmed TJ, Stavrov D, Bersee HEN, and Beukers A. Induction welding of thermoplastic composites an overview, *Composites Part A: applied science and manufacturing*, pp. 1638—1651, 2006.
- [8] Vankan WJ, Hoorn N van, Wit AJ de, and Maas R. Modelling and simulation for innovative aeronautic developments, *proc. Eurogen 2023 conference*, Chania, Greece, 1–3 June, 2023. NLR-TP-2023-183.
- [9] Simulia. https://www.3ds.com/products-services/simulia/products/abaqus/.
- [10] Ambrell. https://www.ambrell.com/.

ELECTROMAGNETIC INDUCTION HEATING OF TP-CFRP LAMINATES

- [11]Wit AJ de, Hoorn N van, Straathof L, Vankan WJ. Numerical simulation of inductive heating in thermoplastic unidirectional cross-ply laminates, *Front. Mater.*, *Sec. Polymeric and Composite Materials*, vol. 10, p. 1155322, Apr. 2023, doi: 10.3389/fmats.2023.1155322.
- [12]Toray Advanced Composites. https://www.toraytac.com/.
- [13] Mathworks. https://nl.mathworks.com/products/matlab.html.
- [14]Koenis TPA, Wit AJ de, Maas R, Hoorn N van. A machine learning approach to dynamic simulation of electromagnetic heating, *ECCM21 21st European Conference On Composite Materials*, Nantes, France, 02-05 July 2024.
- [15]Moser L. Experimental Analysis and Modeling of Susceptorless Induction Welding of High Performance Thermoplastic Polymer Composites, PhD thesis, 2012.